Rain Characteristics in Tropical Regions: Measurements from Radars and Ground-based Instruments

Jun Tan and Carron L Wilson

Radio Communications Research Unit
Rutherford Appleton Laboratory, Chilton, Didcot, Oxon OX11 0QX, United Kingdom
Email: j.tan@rl.ac.uk, Tel: +44-(0) 1235-445758, Fax: +44-(0) 1235-446140

1. Introduction

It is widely known that Earth's climate is affected in part by complex interactions between the Sun and the planet's vast expanse of ocean waters. Understanding their dynamics, and the subsequent formation of water vapour, clouds, rainfall and the release of "latent heat" high into the atmosphere, which then affects global atmospheric circulation, are central to understanding the climate system. For this reason, Earth scientists have been very keen on studying ocean storms and measuring rainfall. The current Tropical Rainfall Measuring Mission (TRMM) project operated jointly by NASA and NASDA is a link in that understanding the tropical water cycle (*Simpson* et al., 1988). Up to now, meteorologists have studied rainfall patterns over the land for more than 20 years using ground- based radar, special aircraft instruments and weather ground stations. Now, for the first time with TRMM, they are able to make extremely precise measurements of rainfall over the ocean, where conventional ground-based instruments cannot see.

Since its successful launch into its orbit in November 1997, the vast amount of data recorded and transmitted back to the earth daily from the TRMM satellite is currently providing us with further evidence on the quantity and structure of tropical precipitation. Consequently, the access of the European scientific community to TRMM data leads to an exceptional opportunity to test the impact of improved measurements of the global precipitation on the numerical weather prediction. As a result, an European Commission (EC) funded research-development program EuroTRMM has been commissioned. The objective of EuroTRMM project is twofold, (1) to process the TRMM data and products in order to provide assimilation data, or verification data for a numerical weather prediction (NWP) model; and (2) to attempt assimilation of the precipitation data in a NWP model, and to use the precipitation data for testing and tuning schemes for parameterisation of convection.

Currently, the rain-retrieval algorithms used in TRMM data analysis depend on several parameters, including melting layer heights and the coefficients relating reflectivity to rainfall relationships. In support of the EuroTRMM project of "Exploitation of TRMM Data for an Improved Weather and Climate Forecast", the Radio Communications Research Unit (RCRU) at the Rutherford Appleton Laboratory (RAL) has designed, built and installed an S-band polarisation-diversity Doppler radar at the Nanyang Technical University in Singapore. The radar has been operated since 1998 in Singapore to record various modes of scanning data. Prior to this, the RCRU has also designed and built a vertically pointing polarisation-diversity S-band radar and operated it in Papua-New Guinea (University of Lae) for almost a year. In addition to the radars, a Joss distrometer was installed at both sites allowing comparison of the drop size distribution measured to the radar derived quantities. At the Singapore site, additional instruments include a rapid-response raindrop-counting raingauge and a logging beacon receiver for the INTERSAT beacon at 12 GHz.

The aims of our projects is to study the characteristics of tropical rainfall by analysing radar data and ground instrument measurements so that we can better understand the evolution of rain events, melting layer heights to obtain the accurate coefficients for estimating rainrates from radar measurements.

2. Descriptions of Radars and Ground-based Instruments

During the EuroTRMM project, the Radio Communications Research Unit (RCRU) of the Rutherford-Appleton Laboratory (RAL) has designed, built and installed an S-band polarisation-diversity Doppler radar at the Nanyang Technical University of Singapore (*Eastment,* et al 1995). The RCRU has also proposed to make use of an existing dataset from a vertically pointing polarisation-diversity S-band radar located in Papua New Guinea (Univ. of Lae) The goals of our study on tropical rain in EuroTRMM project are:

- Calibration and Rainrate Algorithm Validation.
- DSD vertical structure characterisation via Doppler radar spectra and distrometer.
- Convective/Stratiform event identification and frequency of occurrence using LDR as identifier.
- More melting layer height statistics using the LDR parameter as tracer.
- Tropical precipitation measurement for characterising radio propagation conditions in the tropics, building on database of measurements from a Papua New Guinea installation.

In addition to the radars, a Joss distrometer was installed at both sites allowing comparison of the drop size distribution measured to the radar derived quantities (Z_H, N_0, D_0). At the Singapore site, additional instruments beyond the radar and the distrometer include a tipping bucket raingauge and a logging beacon receiver for the Intelsat beacon at 12.75GHz.

2.1 The Radars

The data sets used for this work package come from two sites and two S-band polarisation diversity radars (one at each site) as described in Table 1. The two sites are the Nanyang Technological University campus, Singapore and the University of Lae campus, Papua New Guinea (PNG). The two radars have essentially identical characteristics and the primary difference is the scanning capability of the Singapore radar. The PNG radar consisted only of a fixed pointing (vertical) dish, whereas the Singapore radar has the same diameter dish but mounted on a mechanically-driven positioner, allowing full hemisphere volume scans potentially.

The scanning radar system (Singapore) currently measures and records reflectivity (Z_H), linear depolarisation ratio (LDR), radial velocity (v_r), and velocity spectral width (σ_v) at a ß 1.6 second update rate. A special pulse recording mode is occasionally used to record Doppler spectra if the radar is pointing at zenith, thus giving us an estimate of drop size distributions as the raindrops fall. Both systems use a PC-based data acquisition and radar control system.

The vertically pointing PNG radar system measured and recorded the same parameters as the scanning radar above. However, it only operated for one year during 1996 and so there is no possibility of direct comparison to TRMM data. However, due to the simpler system (non-scanning) it needed less attention and provides an uninterrupted record for 1996 in terms of precipitation profiles and drop size distributions.

	PNG	Singapore
Location	University of Lae campus, Lae, Papua New Guinea (6.40S, 147.2E), now defunct.	Nanyang Technical University of Singapore, building roof of EEE (1.38N, 103.7E).
Scan capabilities	Fixed pointing vertically	Complete hemisphere
Wavelength (cm)	9.87	9.87
Frequency (GHz)	3.03	3.03
Dish diameter (m)	3	3
Disk Gain (dBi)	36.5	36.5
Beamwidth (deg)	2.3	2.3
Pulse length (μs)	1.0	0.5
Peak power (kW)	600	700
Polarisation diversity	Via receiver switcher	2 independent receiver channels
Measurables	Z_H, LDR, v_r and σ_v	Z_H, LDR, v_r and σ_v

Table 1: Radar hardware specifications for PNG and Singapore systems

Photograph and map of the installed 3-meter dish for the scanning radar at NTU, Singapore are shown in the following Figure 1 & 2.

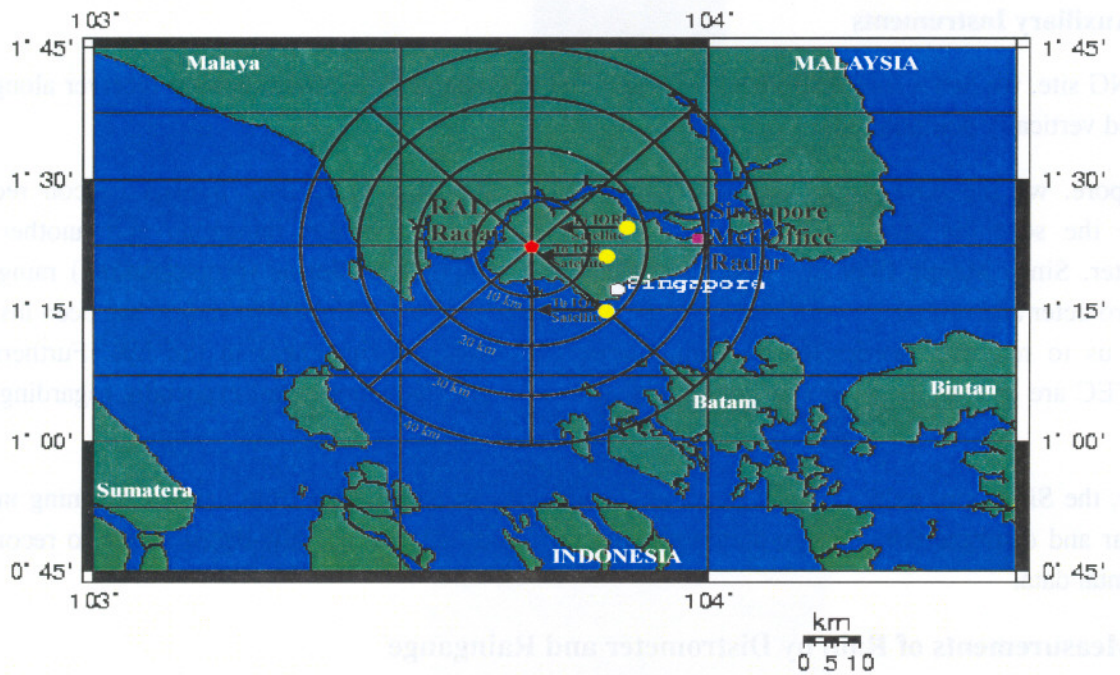

Fig 1: Map of the installed radar system at NTU in Singapore.

Fig 2: Photograph of the installed 3-meter dish for the Singapore radar system.

2.2 Auxiliary Instruments

At the PNG site, we had a Joss distrometer (RD-69) and a Ku-band (12.75GHz) beacon receiver along side the S-band vertically pointing radar.

In Singapore, we the have same Joss Distrometer and a Ku-band (11.2GHz) Intelsat beacon receiver alongside the scanning radar. NTU separately operate a tipping bucket raingauge and another Joss Distrometer. Since March 1999, we have installed a fine temporal resolution (drop-counting) raingauge. Both distrometer and raingauge are sampling at 10 seconds. Moreover, a Unix workstation has been installed to allow us to remotely access the data and view it in near real time here in the UK. Furthermore, ESA/ESTEC are to loan us a video distrometer that should give us better detail especially regarding drop size.

Currently, the Singapore radar is being operated 24 hr a day to record data from various scanning modes. Both radar and distrometer/raingauge data are being mirrored daily on our UK-based server to record the experimental data.

3. Measurements of Rain by Distrometer and Raingauge

The Joss distrometer, which logs data continuously, has a cross-sectional area of 50cm^2 and records drops between 0.3 and 5mm in diameter size. The integration time used in this study was 60 seconds and to reduce sampling errors rainfall rates of less than 0.1mm/hr have been excluded from the analysis. The same Joss distrometer was deployed in both Singapore and PNG. For Singapore site, a rapid-response drop counting

raingauge has been installed to measure rainfall rate. The sampling time is 10 seconds and integration time is also 60 seconds.

Examples of raingauge and distrometer measurements in two rain events are shown in Figure 3 (a)-(b).

(a)

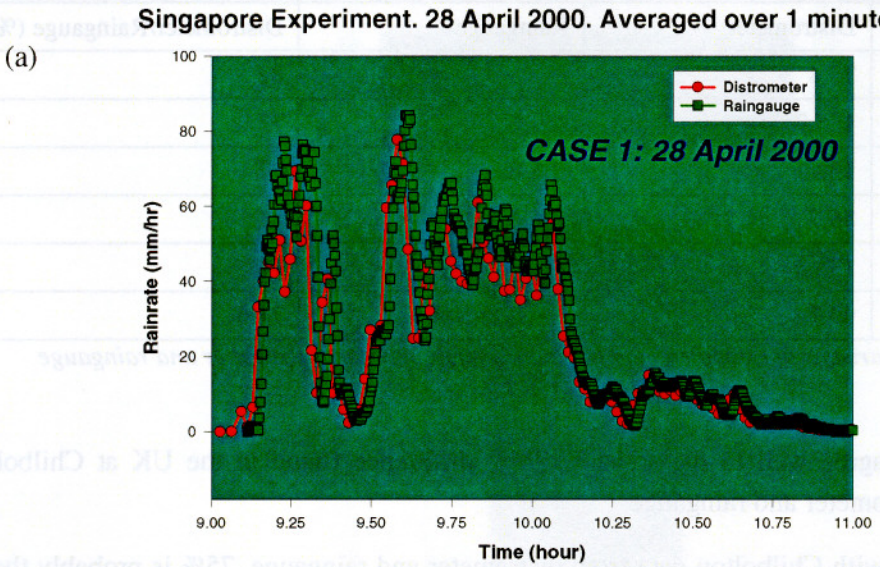

(b)

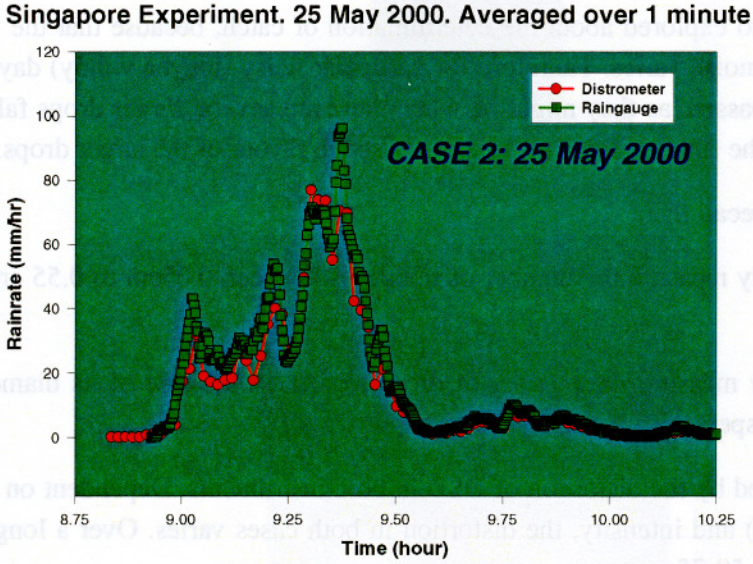

Fig 3(a). Rain event recorded on 28 April 2000.
Fig 3(b). Rain event recorded on 25 May 2000.

Apparently, as seen in Figure 3(a)-(b), there are good agreements in estimated rainrates between distrometer and raingauge. However, the monthly-accumulated rainfall estimated from these two instruments tells a different story.

Month in 2000	Estimated monthly-accumulated rainfall (mm)		Difference
	Distrometer	Raingauge	Distrometer/Raingauge (%)
May	72.4	87.6	82
June	125.9	171.7	73
July	158.7	206.2	77
August	86.7	106.6	81
September	135.3	177.6	74
October	99.7	133.7	74.6

Table 2: Comparisons of estimated monthly total rainfall between distrometer and raingauge

The above comparisons agree well to the so-called 75% difference found in the UK at Chilbolton with estimated rainfall by distrometer and raingauge.

Based on our experience with Chilbolton data from distrometer and raingauge, 75% is probably the best we have seen in comparisons between our drop counting gauges and the Joss impact distrometer. The average findings are much lower than that, down around 50%. This is both when comparing accumulation results and rainfall rate peak intensities. Some differences may be explained by coincident drops but this probably would not explain all of the differences.

The effect of wind can also explored about the determination of catch, because that the noise ratio of what the distrometer ignores as noise varies. Therefore for particular noisy (maybe windy) days the impact of the smaller drops may be surpassed, as they might be when there are several larger drops falling in a particular event again the impact of the smaller drops may be surpassed in favour of the larger drops.

One the other hand, if we recall that

(1) Distrometer will only measure the number of raindrops between 0.05cm to 0.55 cm diameter over 20 channels

(2) Raingauge will only measure the number of drops regardless the size of its diameter. Essentially, it measures a mono-dispersal drop size distribution

So the errors may be caused by the distortion of DSD in both instruments. Dependent on the type of rainfall (convective and stratiform) and intensity, the distortion in both cases varies. Over a long-averaging period, we may get something like 50-75 percent.

While the Singapore radar has been calibrated with our Chilbolton advanced 3 GHz polarisation-diversity radar before it was installed in Singapore, it is pleased to confirm the system calibration tend to be stable when using distrometer data to simulate radar reflectivity and compare with radar measured reflectivity, the agreement confirms the range of our system calibration, as shown in Figure 4. In the Figure, radar measured reflectivity from vertically pointing scan and 44° elevation fixed scanning is labelled as (vertical) and (44°), respectively.

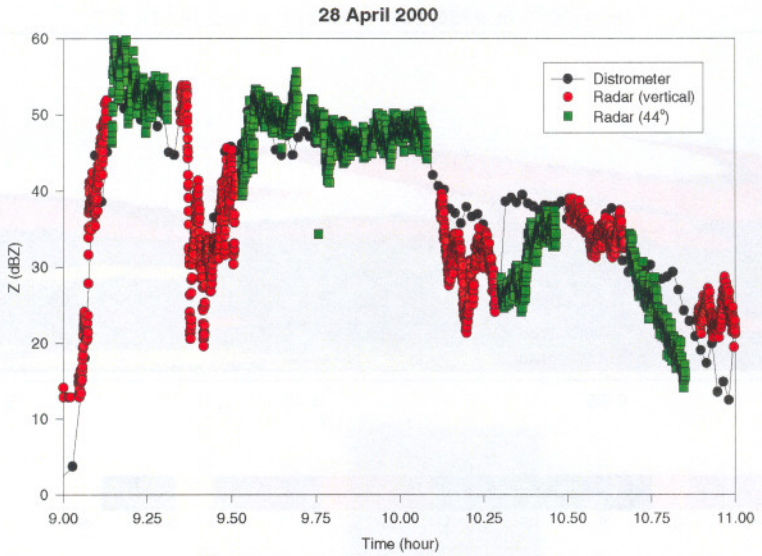

Fig 4. System calibration for Singapore radar using distrometer data

4. Classification of Rain and Evolution of Z-R Relationship

4.1 Classification of Rain Events

Re-examining rainfall rates shown in Figure 3(a)-(b), we can find that both events start as convective storm and they gradually become weak and finally they develop as stratiform storm. Corresponding measurement from radar reflectivity shows similar description, as shown in Figure 5 (a)-(b).

The events from Singapore were not only classified into convective and stratiform regions, as in previous studies in PNG (Ladd et al, 1997), Tokay and Short (1996) (TS) and Atlas et al (1996), but were also split into two more regions; initial convective and transition. The transition section, lying between the convective and stratiform regions, is becoming more widely used in tropical classification (Atlas et al, 1998 and Black et al, 1997).

To classify the distrometer data gathered in Singapore the criteria laid down by Atlas et al (1998) were utilised along with detailed analysis of the radar data. The four sections were categorised as follows.

1. In the first section, the initial convective region, there is a sharp increase in the rain rate (R) but D_O does not vary greatly.

2. The convective section follows on until just after the maximum peaks in R, reflectivity (Z) and D_0, where D_0 starts to decrease rapidly and R is less than $0.6R_{MAX}$. The corresponding radar data shows large updrafts occurring during this period, represented by negative motions on the velocity profiles.

3. The third section, the transition, is the trailing portion of the convective section where Z and R decrease in unison with D_0.

4. This then moves onto the final section of the event, the stratiform region, characterised by the presence of a bright band (the melting layer) in the radar data and a decrease in the downward velocity. D_O starts to increase again and the rain rate stays at a roughly constant level, less than 10 mm/hr. The event finishes when all three parameters, Z, R, D_0 start to decrease.

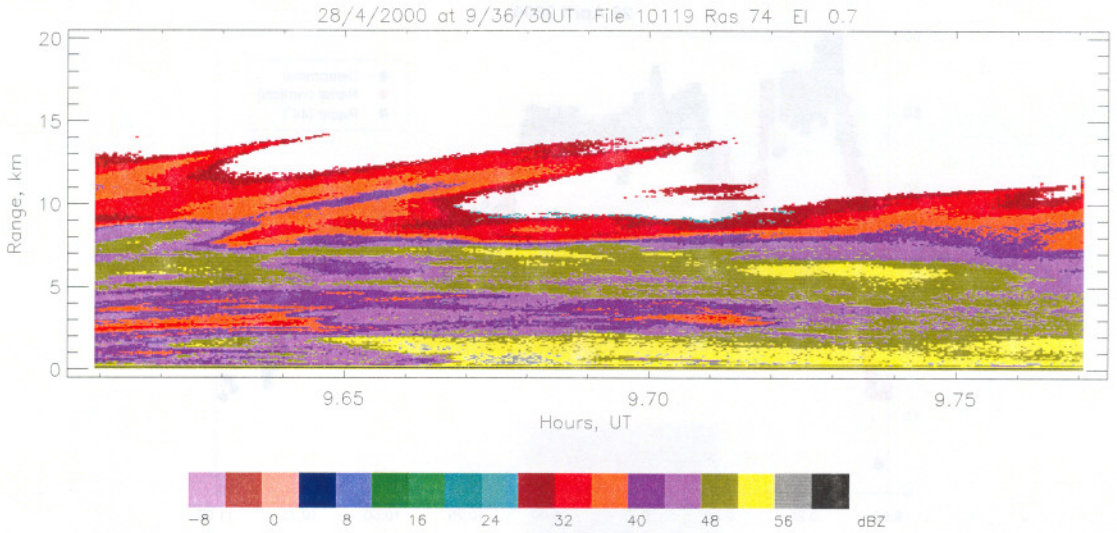

Fig 5(a). Vertically Pointed Scanning: Evolution of rain/radar reflectivity from convective to stratiform as recorded on 28 April 2000 by Singapore S-band radar

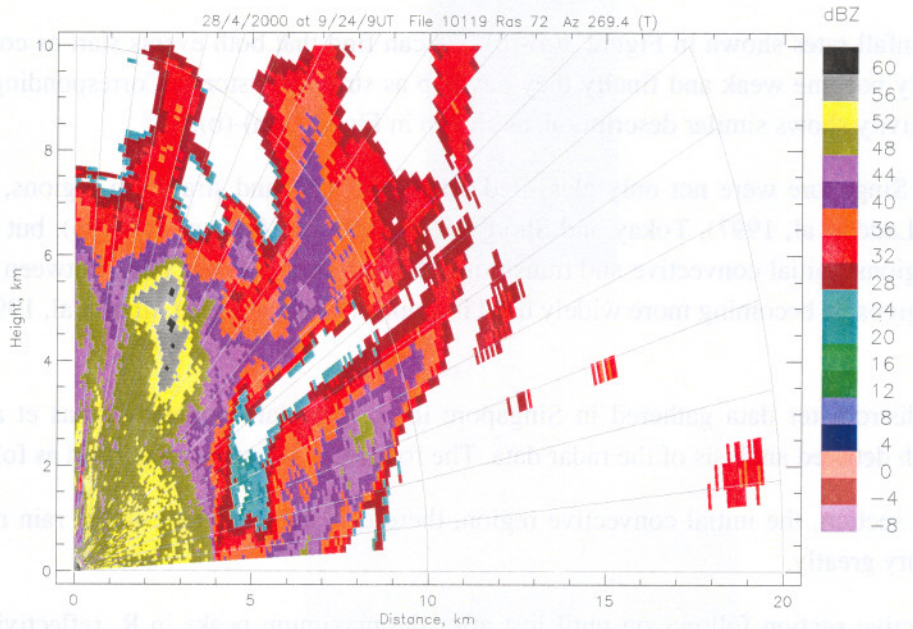

Fig 5(b). RHI Scanning: Evolution of rain/radar reflectivity from convective to stratiform as recorded on 28 April 2000 by Singapore S-band radar

Five major events that occurred between June 1998 and December 1998 were examined in this study. Each were classified into the four sections, an example of which is shown in Figure 6 along with fixed vertically pointing radar data for the same day (Fig. 7).

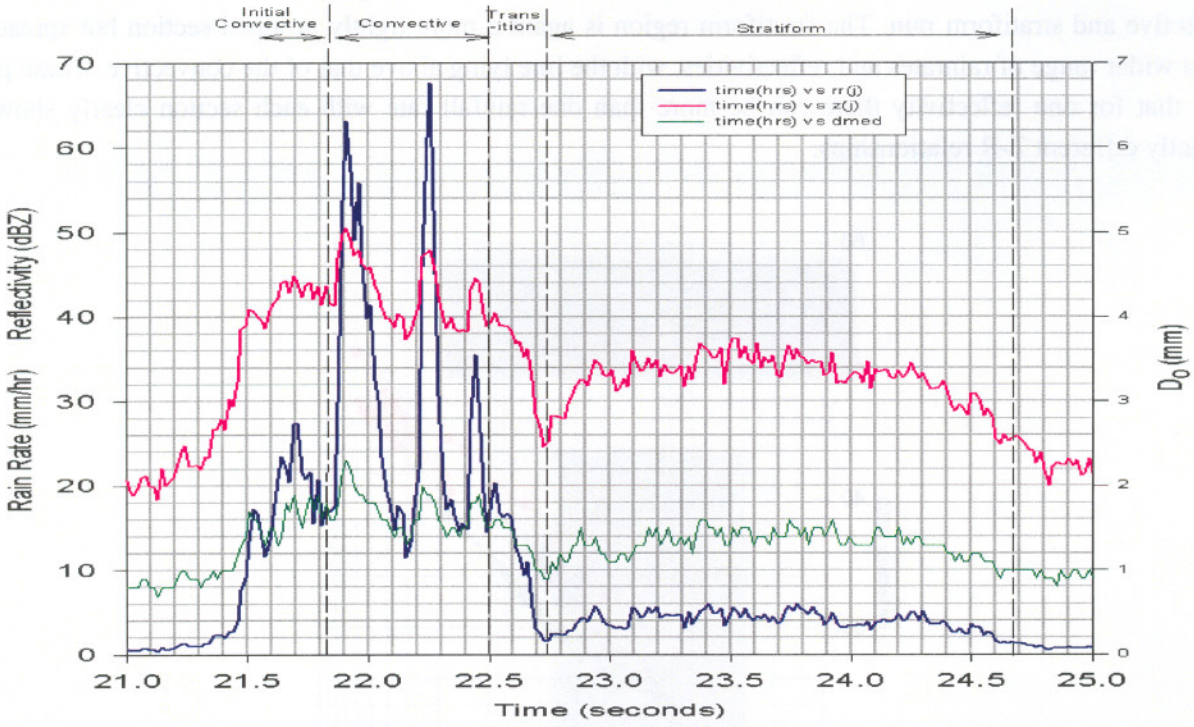

Fig 6. Example of classification of rain events for data recorded on 9 June 1998 in Singapore

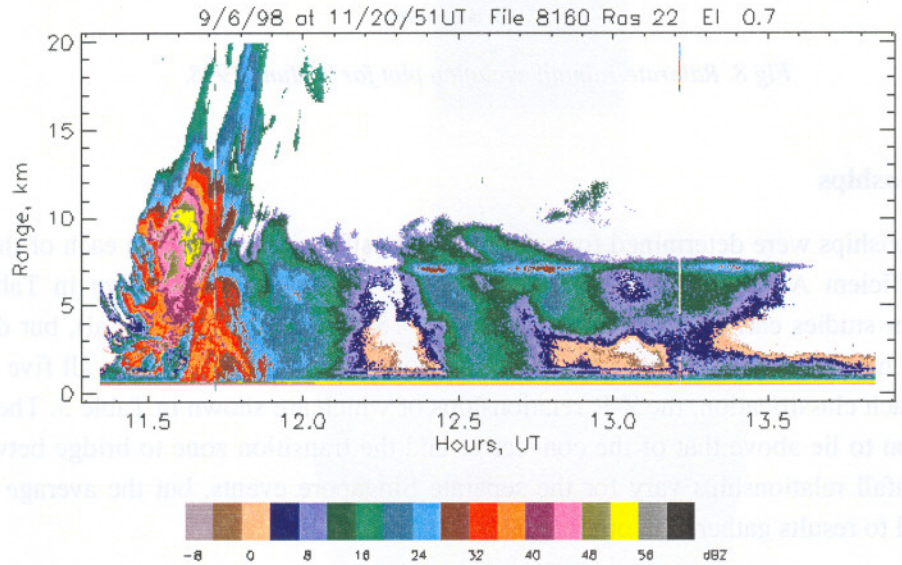

Fig 7. Radar reflectivity for the fixed vertically pointing radar data recorded on 9th June 1998 in Singapore

4.2 Reflectivity - Rainrate Evolution

Data plots of reflectivity against rain rate show a systematic trend through the four sections of an event. These can be useful in aiding the classification of the different regions, especially if no radar data is available. One such event is shown in Figure 8 from the 9th June 1998. The event shows a sharp increase in Z and R during the initial convective section, leading up to the tightly clustered convective section with high

rainfall rates. This then decreases in reflectivity and rainfall rate during the transition zone between the convective and stratiform rain. The stratiform region is again a more tightly grouped section but spreading over a wider range of rainrates and reflectivities, with the line lying above that of the convective. These plots show that for one reflectivity there can be more than one rainfall rate with each section clearly showing distinctly different Z-R relationships.

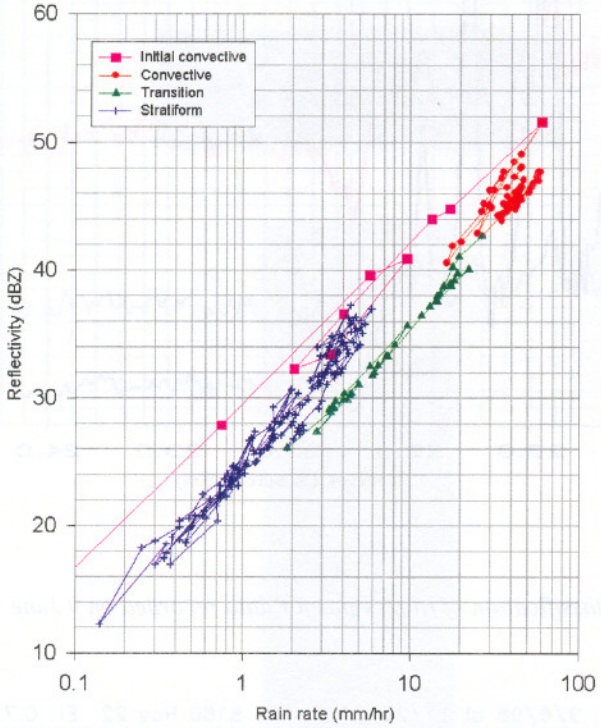

Fig 8. Rainrate-rainfall evolution plot for 9th June 1998.

4.3 Z-R relationships

Separate Z-R relationships were determined for each of the classification sections in each of the events. The values of the co-efficient A and exponent b for the $Z=AR^b$ relationship are shown in Table 3 and are consistent with other studies carried out in the tropics (e.g. TS, Atlas et al, Ladd et al), but differ to those from temperate and mid-latitude climates. The graph in Figure 9 shows the data from all five events, along with curve fits on each classification, the Z-R relationships of which are shown in Table 3. The results show the stratiform section to lie above that of the convective and the transition zone to bridge between the two. The reflectivity-rainfall relationships vary for the separate Singapore events, but the average from all five events compare well to results gathered in other regions.

The Z-R relationships for PNG, TS and Singapore are very similar, TS's convective Z-R has a greater bias towards the curve fit relationship from the transitional region of the Singapore data, rather than the convective section.

Atlas et al (1998) previously stated that past convective relationships are often closer to the transitional section. Until recently there were only two classifications for tropical events, convective and stratiform regions, and the majority of the data from this newly classified transitional section would have been classified as convective, particularly as there is no bright band.

	Convective		Transition		Stratiform	
$Z=AR^b$	A	b	A	b	A	B
Sing. Daily events						
9_6_98	583.79	1.14	134.55	1.44	294.23	1.49
24_9_98	67.33	1.68	350.55	1.05	353.65	1.30
23_10_98	1271.1	1.04	387.74	1.29	337.36	1.27
7_12_98	519.78	4.70	121.22	1.51	334.77	1.60
26_12_98	80.62	1.66	136.67	1.44	131.56	1.98
Singapore, averaged	***138.98***	***1.50***	***270.53***	***1.25***	***330.03***	***1.35***
TS (1996)	*139.00*	*1.43*	NA	NA	*367.00*	*1.30*

Table 3. Reflectivity-rainfall relationship co-efficients, $Z=AR^b$

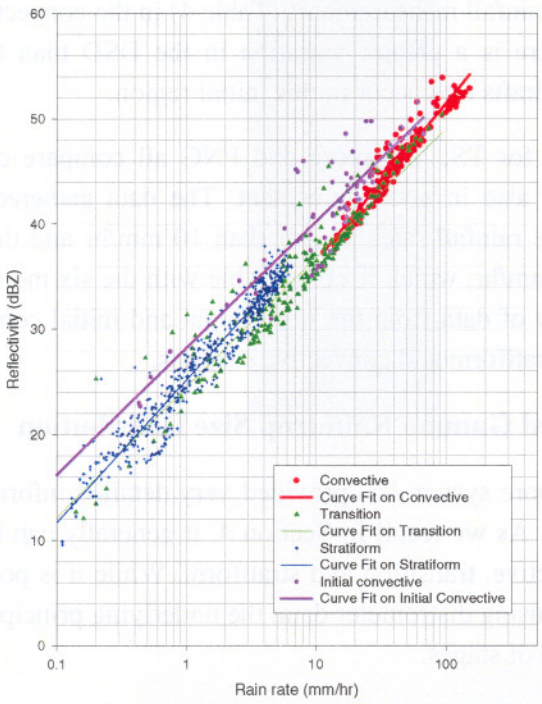

Fig 9. Z-R fits for each of the four classifications for all five major Singapore events

	Singapore Z-R	TS Z-R
Convective	0.67	0.98
Transitional	0.19	0.33 (using TS convective Z-R)
Stratiform	0.32	0.33

Table 4. Fractional standard deviation to compare R calculated from either Singapore Z-R or TS Z-R derived relationships with original rainrates measured by the Joss distrometer in Singapore

During the transitional period, if the Singapore transitional Z-R and the TS convective Z-R relationships are compared, the results show the Singapore data to have a negative bias and TS to have a positive bias, with both comparing well to the original rainrates (see Table 4). The results show the TS convective Z-R to have a 33% error from the original rainrates, which is nearly a third of that for the comparison with the Singapore convective data. This is in agreement with the Atlas et al (1998) finding that Z-R convective relationships often work well on transitional events. Atlas et al (1998) also states that this "mistaken inclusion of transition rain within the convective class leads to a serious error in the apportionment of the diabatic heating and cooling".

If we compare the two convective Z-R relationships, from TS and Singapore, with that of the original convective classified rain, and calculate R from the distrometer derived reflectivity's, the results again show that the Singapore Z-R has a negative bias but compare better than that which is calculated from the TS convective Z-R, which tends to overestimate R. TS has a 41% error for R with a greater than 20% error from the original rainrates, which is more than double that of the error from the Singapore Z-R calculated R. In heavy precipitation in the convective region the TS convective Z-R relationship on occasions overestimates the rainfall by greater than 40 mm/hr. Both the Singapore and TS convective Z-R relationships have a greater than 65% error from the original rainfall measurements (Table 4) in the convective region. This large error is because in convective events there is a greater variation in the DSD than that of the stratiform region, because of the updrafts and downdrafts that occur in this initial region.

The stratiform Z-R relationships for TS, Singapore and PNG all compare closely. The rainrates for the separate event classifications are also in good agreement. The data gathered in Singapore show that all convective classified regions have rainfall rates greater than 10 mm/hr and that all stratified sections have rain rates less than or equal to 6 mm/hr, which is comparable with the six months of data collected in PNG, and with that of TS. The majority of data from the transitional and initial convective regions can be found between the rainfall rates of the stratiform and convective sections.

5. Exploring a Normalised Gamma Raindrop Size Distribution

Radar measurements from Singapore system has provided very detailed information about the evolution of rain storm within a given period.. As we recall in Section 4, it generally can be classified into four stages, namely, initial convective, convective, transition and stratiform. While it is possible to obtain different Z-R relationship for different stage by using distrometer data, the underlying principle is to model such a raindrop size distribution that it fits all kind of stages.

As we know, raindrop size distributions are not perfectly exponential and are better represented by gamma functions with three variables No, DO and μ as a measure of their concentration, mean size and breadth, respectively. If rainfall rate, R, e.g. is derived from reflectivity, Z, alone, then variations in drop spectra lead to errors in R of up to a factor of two. On the other hand, the polarisation radar parameters such as differential reflectivity (ZDR), and specific differential phase shift (KDP), should better define the drop size distribution and lead to more accurate estimates of rainfall, R, than from Z alone. The use of non-normalised gamma functions leads to apparent relationships between μ and No and between μ and the exponent b in $Z=aR^b$. The values of a and b have been used to predict the ranges of No Do and μ in naturally occurring rain, and therefore to derive empirical relationships between R and Z, ZDR and KDP to provide more accurate estimates of rainfall rate. When normalised gamma functions are used, these relationships are no longer true, and the range of No, Do and μ cannot be derived from a and b.

Basically, normalised raindrop size distribution is defined as

$$N(D) = N_0^* F(D / D_m) \tag{1}$$

$F(X)$ is the desired function of $X=D/D_m$, in which is expressed as "normalised DSD"

Steps to calculate normalised DSD from distrometer data are given in Testud et al (2001)

1) Calculate M_3 and M_4 moments of DSD, where M_n is defined as follows

$$M_n = \int N(D) D^n dD \tag{2}$$

2) Calculate $D_m = \frac{M_4}{M_3}$

3) Calculate $N_0^* = \frac{4^4}{\Gamma(4)} \cdot \frac{M_3^5}{M_4^4}$

4) Calculate $F(X_i) = \frac{N(D_i)}{N_0^*}$ for all drop sizes

5) Best fitting $F(X_i)$, e.g., modified exponential (see J. Testud et al, 2001)

Using the distrometer data from the same event we described in Figure 5(a)-(b), we can derive the relevant normalised Gamma DSD parameters. These parameters are plotted in Figure 10.

To examine the grouping behaviour, we plot all the data into clutter as shown in Figure 11. Clearly, we can see that there is a very good power relationship between the R / N_0^* and D_m. This is essentially the foundation for using normalised Gamma DSD to model raindrop.

To obtain a best fitting normalised Gamma DSD, we propose a scheme to classify all rainrates into the following three regions:

- R > 30 mm/hr (shown in Figure 12 as symbol ◊)
- 30 > R > 10 mm/hr (shown in Figure 12 as symbol Δ)
- R < 10 mm/hr (shown in Figure 12 as symbol □)

Then we have adopted the modified exponential function suggest by Testud et al (2001), which is defined as follows

$$F(X) = \exp(a - 4X - s\sqrt{(X - X_0)^2 + b}) \tag{3}$$

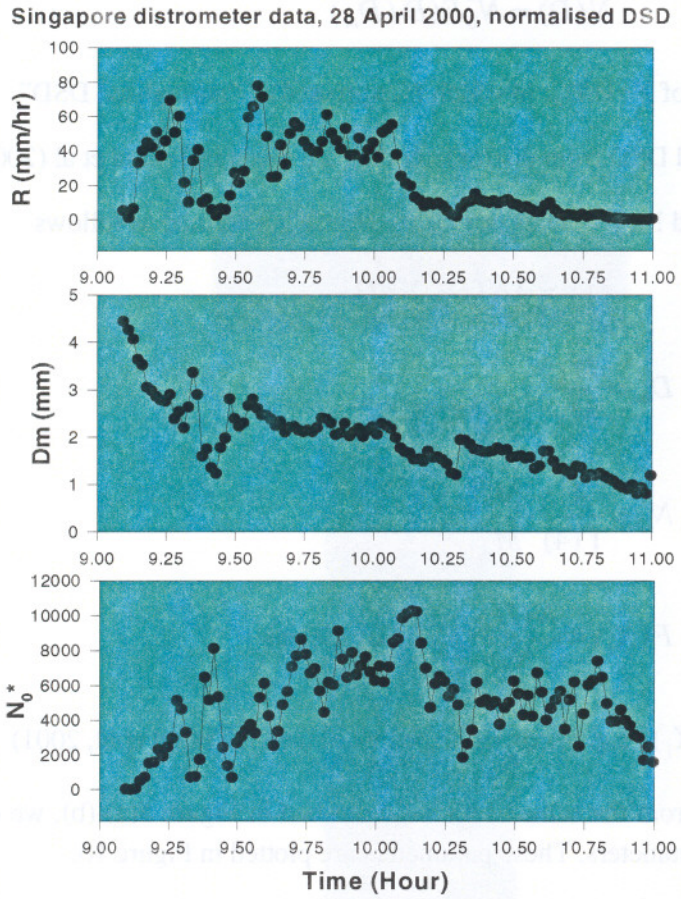

Figure 10. Derived normalised Gamma DSD parameters for distrometer data recorded on 28 April 2000 in Singapore.

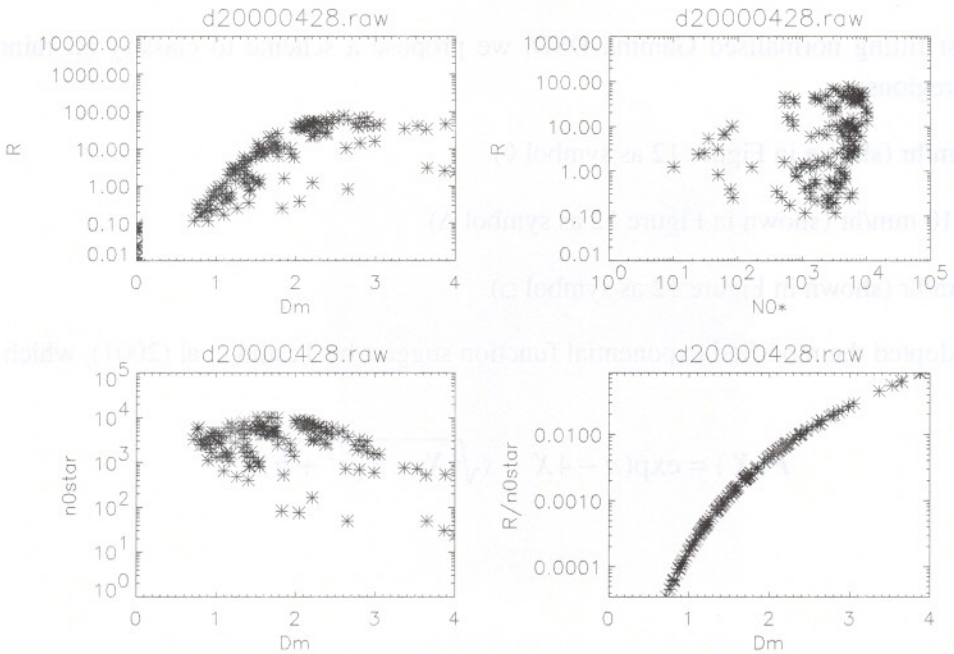

Fig 11. Clutter plots of various normalised Gamma DSD parameters.

Where the two parameters *s* ("slope") and *b* ("smoothness") may be fixed a priori, while the two others *a* and X_0 are to be determined from the first two in order to respect the normalisation. Good combinations to fit the TOGA-COARE data as suggested by Testud et al (2001) are:

- *s = 1.5; b = 0.06;* X_0 *= 1.124; a = 0.705*
- *s = 2; b = 0.06;* X_0 *= 1.111; a = 0.912*

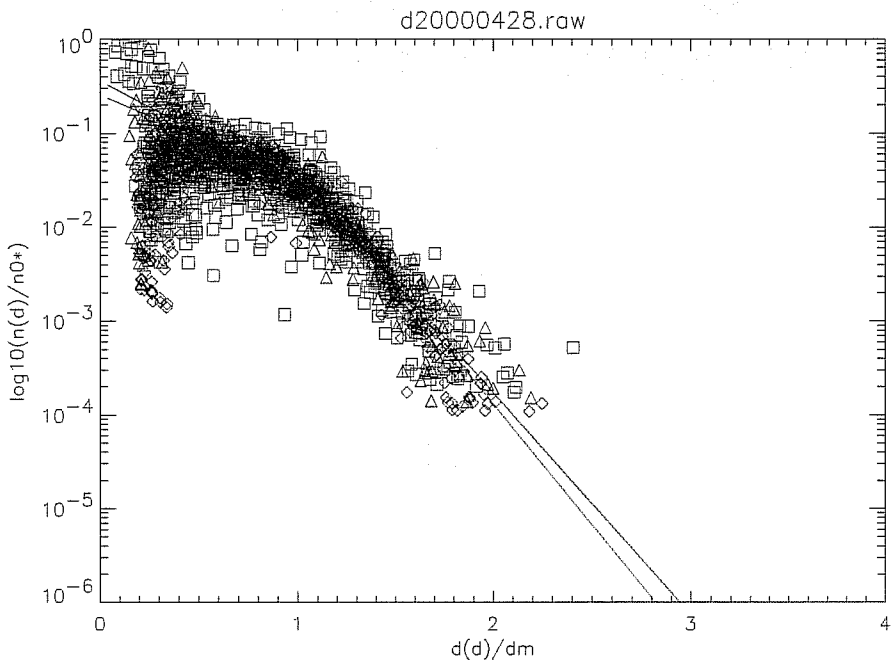

Fig 12. Comparison between Best-fitting normalised Gamma DSD and measurements from distrometer in Singapore.

As can be seen in Figure 12, the agreement between the best fitting and distrometer is at its best for medium to large raindrop, there seems to be a large disagreement for small drops. This may be caused by the truncation effects of limited dropsize measurable by Joss distrometer (0.3 mm). Nevertheless, either fitting seems to provide a good description of all the three regions of rainfall rates. Further work will be focused on more case analysis and comparisons between Singapore, PNG and Chilbolton.

6. Melting Layer Heights and Thickness

The heights of melting layer bottom and top (i.e., rain height and melting thickness) have been derived from the vertical profiles of radar parameters of S-band radar measurements in Singapore.

The melting layer is the transition region between snow and rain, it usually starts at the 0°C-isotherm level and finishes at a few degrees above 0°C where all the snow particles have melted and become raindrops. The information regarding its height and thickness are vitally important to both remote sensing and radiowave communications research because it can lead to the total raincell height and the impact of melting particles. As active devices, radars have been used to study the microphysical properties of the atmosphere since World War II. The observation of the melting layer in radar parameters gives rise to bright band signatures, which are caused by a high concentration of particles of high index of refraction arising from the melting snow, with the additional factor of non-spherical shapes. An example of radar measurements recorded in

Singapore for vertically pointing scanning is shown in Figure 13(a)-(b) for radar reflectivity Z, linear depolarisation ratio LDR and Doppler velocity v, respectively.

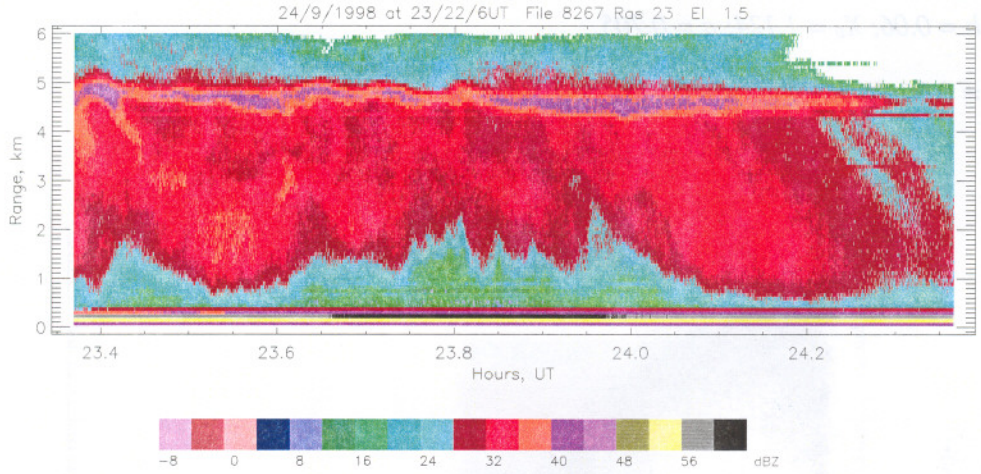

Fig 13(a). Radar reflectivity for vertically pointing scanning in Singapore

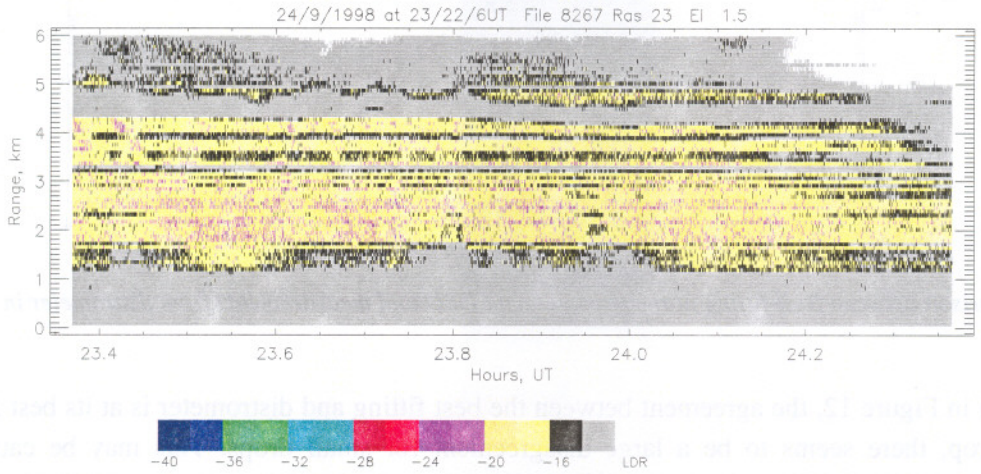

Fig 13(b). Radar linear depolarisation ratio for vertically pointing scanning in Singapore

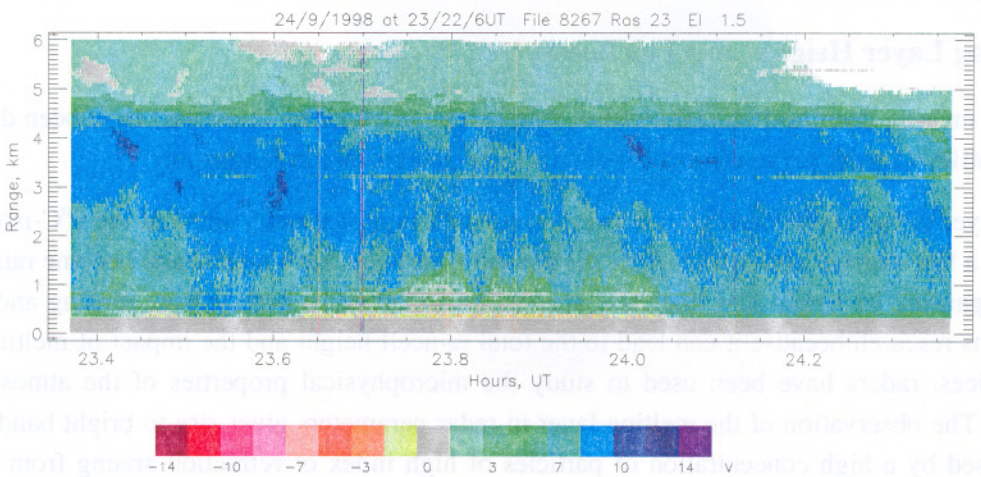

Fig 13(c). Radar Doppler velocity for vertically pointing scanning in Singapore

6.1 Statistics of Melting Layer Heights in Singapore and PNG

The cross-polar and Doppler information from the radar data has been analysed to determine the height of the melting layer in Singapore and PNG. The graph in Figure 14 shows the statistical analysis of the melting layer heights during stratiform regions. There is a difference of 300m between the two locations, this relates to the approximate mean temperature difference of about 2 degrees between the two countries during the time periods of data collection. In PNG we were also able to distinguish a melting layer height during some of the convective events; this varied between 3 and 8 kilometres. The maximum height of the radar echoes occurred during convective events and reached heights of fifteen kilometres above the ground in both locations.

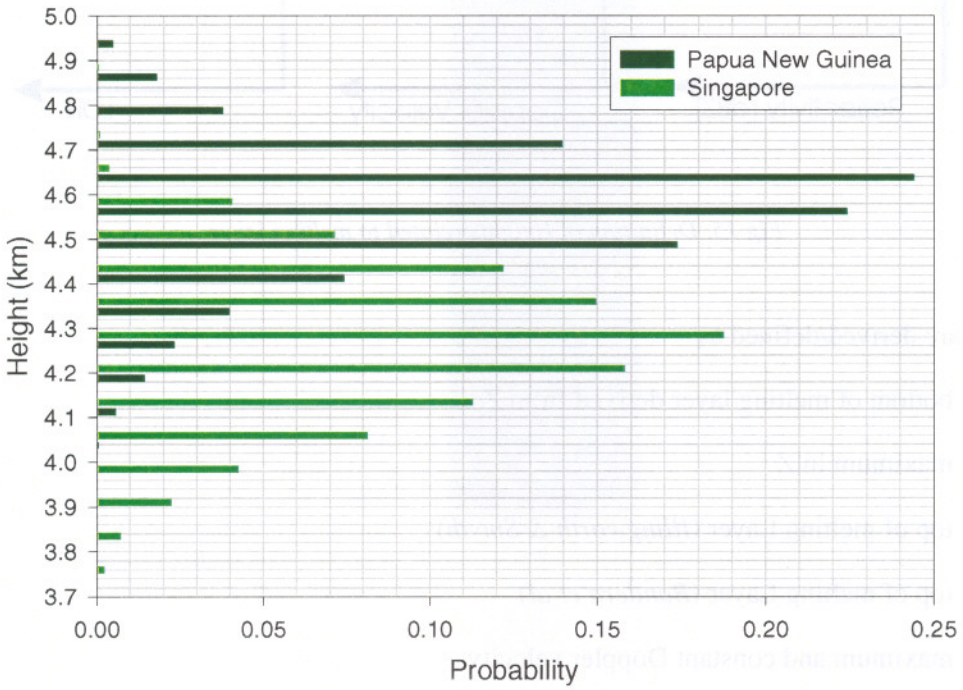

Fig 14. Statistics of melting layer heights in Singapore and PNG.

6.2 Melting Layer Thickness, Heights of Top and Bottom

Utilising the Singapore radar data, we have studied vertical profiles from strong stratiform events during 1998. Six different heights are defined and can be derived from the vertical profiles of dBZ, LDR, and velocity, as shown in Figure 15.

From the reflectivity profile, four measurements were recorded:

- The level above which dBZ begins to increase rapidly, at the bottom of the enhancement.
- The position where the peak in dBZ occurs.
- The point at the top of the enhancement directly above position A, therefore has the same dBZ value as that of point A. This is the referred to as the 'Freezing level point', Smyth and Illingworth, 1999.
- Location where the gradient rises sharply after the enhancement in dBZ, Bandera et. al. 1998.

Similarly, from the Doppler velocity only one point V was noted where the mean Doppler Velocity occurs just after melting (Klassen, 1988) while in LDR, the peak, L, was recorded.

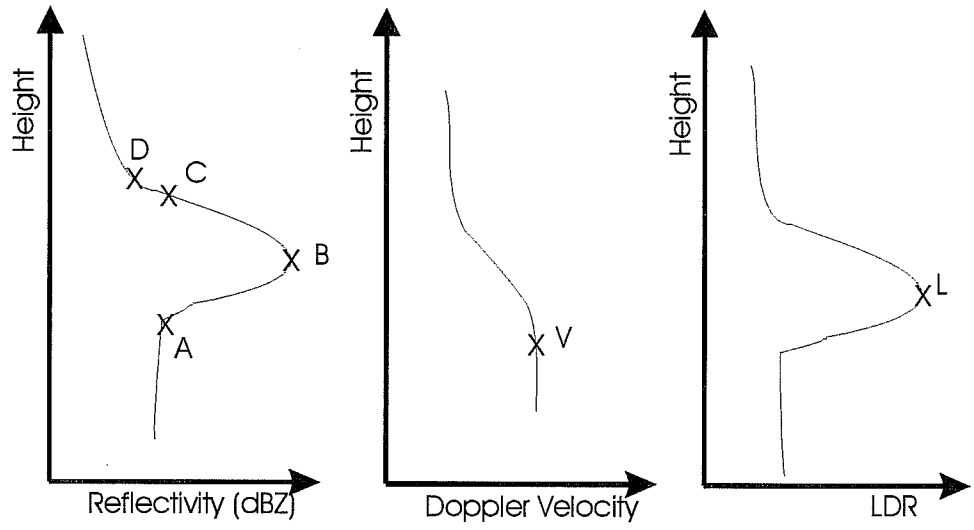

Fig 15. Definition of Heights related to melting layer

Where Heights are derived/defined as

A – bottom of melting layer derived from Z

B – maximum in Z

C – top of melting Layer (*Illingworth & Smyth*)

D – top of melting Layer (*Bandera et al*)

V – maximum and constant Doppler velocity

L – maximum in LDR

O – 0 °C isotherm from radiosonde data

Fifty-six vertical profiles were used in this study, they were recorded between 3rd September and 24th December 1998, during the end of the SW monsoon season and throughout the pre NE monsoon season. The four points; A-D, described in the previous section were recorded for each vertical profile from the radar, an example of an extracted vertical profile taken at midnight UTC is shown in Figure 16. The radiosonde is launched twice daily at the East of Singapore Island (lat. 1.33 deg. N, long. 103.88 deg. E, 14m asl) at 00:00 UTC and 10:00 UTC, and measurements are taken at 50m intervals from ground level to 5500m aloft. Data is only available for the year 1998, and is courtesy of NTU.

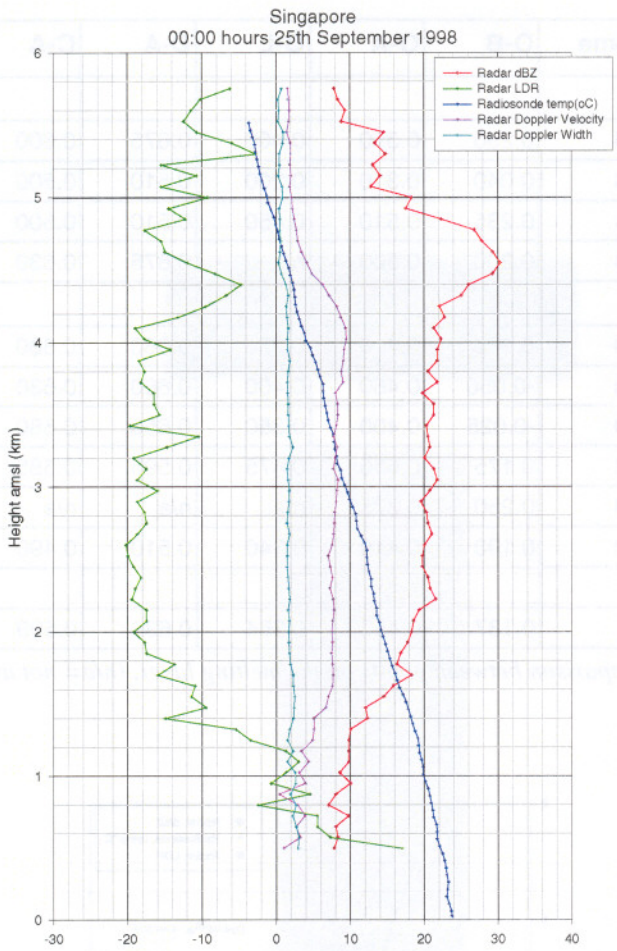

Fig 16. Vertical profiles of radar parameter Vs radiosonde temperature profile.

The thickness of the melting layer varies depending on which point you take as the top, point C or point D, although in both cases the bottom is taken as point A. Taking point C as the top results in a melting layer thickness of between 0.4-1.0 kilometres, with a peak around 0.7 kilometres. While utilising position D as the top results in a melting layer thickness of 0.5-1.3 kilometres thick and a mean of 0.84 kilometres. As expected using points A-D results in a mean melting layer thickness greater than that of A-C.

6.3 Comparisons between radiosonde and radar data

During the period between early September and late December 1998, there were ten stratiform events where both vertically pointing radar data and radiosonde data were recorded, four were in the morning and six in the evening. Comparisons were made between the temperature profiles from the radiosonde data, and dBZ, LDR and Doppler velocity from the radar data. Measurements were recorded for points, A-D, A, V, L and O. The latter representing the zero degree height from the radiosonde data. An example is shown in Figure 17 from the 25th September 1998, while Table 5 shows the comparison between some of the points on the melting layer and Figure 17 shows the average height value for each point amsl.

Date	Time	O-B	O-A	O-L	D-A	C-A	L-A
AM							
25/09/98	24	0.250	0.550	0.400	0.675	0.600	0.150
22/10/98	24	0.040	0.310	0.200	0.510	0.500	0.110
12/11/98	24	0.235	0.510	0.450	0.510	0.500	0.060
27/12/98	24	0.200	0.500	n/a	0.675	0.630	n/a
PM							
24/09/98	10	0.100	0.450	0.220	0.960	0.880	0.230
04/11/98	10	-0.050	0.460	0.400	0.660	0.630	0.060
04/12/98	10	-0.025	0.400	0.350	0.650	0.580	0.050
05/12/98	10	0.175	0.550	0.475	0.595	0.585	0.075
07/12/98	10	0.250	0.375	n/a	n/a	n/a	n/a
08/12/98	10	0.190	0.410	0.340	0.510	0.490	0.070
Average		0.137	0.452	0.354	0.638	0.599	0.101

Table 5. Comparison between points on the melting layer, (n/a= not available).

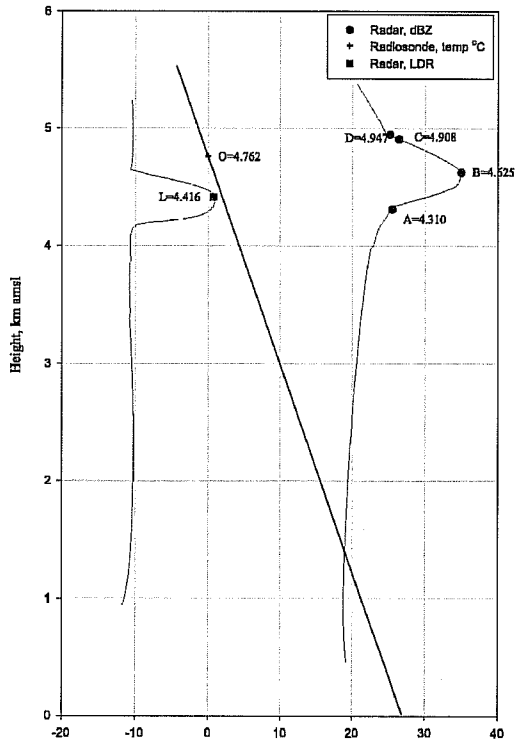

Fig 17. Average values of points, A-D, L & O in the melting layer.

In Figure 17 and the rest of analysis, we have also noticed that the height associated with peak in LDR is lower than the height associated with peak in dBZ. This is due to the difference between the microphysics in dBZ and LDR. On the one hand, dBZ is mainly determined by the size and dielectric constant of hydrometers, on the other hand, LDR is not only determined by the shape and orientation (canting) of

hydrometers but also by the cross-polar return of the non-spherical particles. The height of the peak in LDR is closer to the bottom of melting layer than that of peak in dBZ.

In comparisons between the radiosonde temperature profiles and the radar data, the 0°C isotherm occurs roughly half way between the peak in the melting later and the top of the melting layer, and around 450 metres above the bottom of the melting layer. The average distance between points O and B is 137 metres, this is considerably less than the traditionally used 500m between the 0°C isotherm and the peak in the melting layer.

The bottom of the melting process is taken to be point A, the start of the enhancement in dBZ, average height 4.31 kilometres. This results in a melting layer thickness of around 450 metres, starting at 0°C and finishing at 4-6°C.

The above results clearly illustrate the differences between the heights of bright band and melting layer. The bright-band, namely the observation of melting process is usually associated with the peak/maximum radar reflectivity dBZ, whereas the melting layer is a region of the atmosphere in which particles melt from pure ice to water. There are two heights associated with melting layer, namely, top and bottom. We have found that the height of peak dBZ is usually closer to the top of melting layer whereas the height of peak LDR is closer the bottom of melting layer. In other words, the parameter LDR is a better signature to identify the total rain height

7. Comparisons of Attenuation between Beacon Measurements and Radar-derived

One of the aims of deploying this S-band rain radar is to predict the rain-induced attenuation along the earth-space communications link. To do so, it is critical to have information regarding to rainfall rate along the path, total rain-height and the relationship between rain rate and the specific attenuation. Since the attenuation at S-band is normally negligible, radar data at S-band can be used to predict the total path attenuation.

We have successfully derived information such as storm type, melting layer height and attenuation A-R relationships. Using this information, we have produced an empirical relationship between rainrates and specific attenuation at Ku-band. The coefficients are sensitive to the storm type. The averaged coefficients for convective storm are shown as follows.

$$A = 0.0149R^{1.13} \quad \text{(dB/km)} \qquad (4)$$

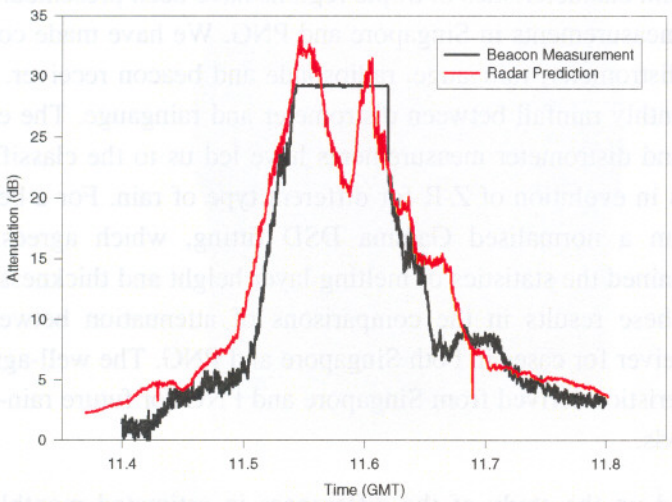

Figure 18 Comparison of attenuation between beacon and radar for 9th June 1998.

From this we can predict attenuation using the rain radar data and compare it with the in-situ beacon measurement. From 1st June 1998, we have pointed the radar along the INTELSAT path for three months. The radar elevation is 44 degrees, the same as the ground-based Ku-band beacon receiver. One comparison is shown in Figure 18 for a convective event recorded on 9th June 1998. Radar measurement of this convective storm is shown in Figure 19. As can be seen, because of heavy rainfall, the beacon receiver saturated between 11.5 to 11.6 hours due to severe attenuation (above 30 dB). The graph shows good agreement between beacon measurements and radar-derived attenuation.

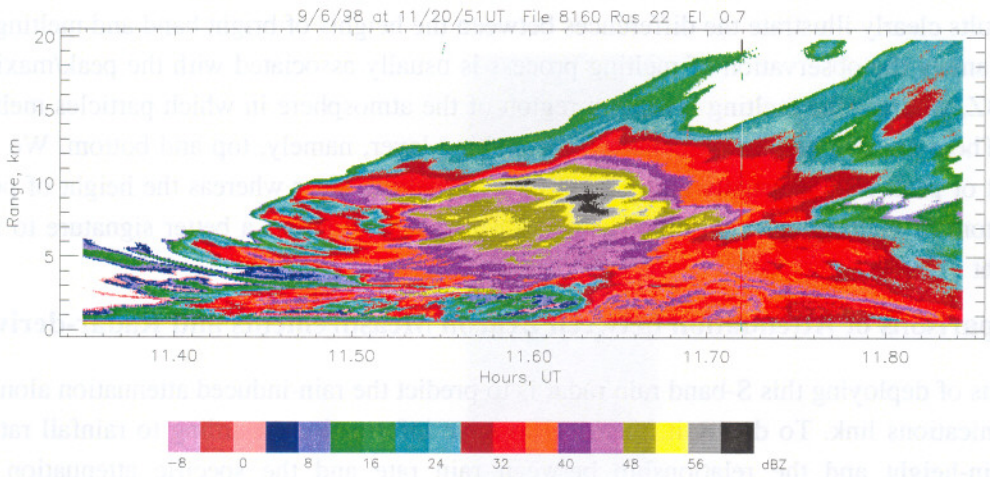

Fig 19. Convective storm recorded by Singapore radar on 9th June 1998.

8. Summary and Future Work

In this paper, results about rain characteristics in tropic regions have been presented. These results have been derived from S-band radar measurements in Singapore and PNG. We have made comparisons with ground-based instruments such as distrometer, raingauge, radiosonde and beacon receiver. We have illustrated the differences of estimated monthly rainfall between distrometer and raingauge. The evolutions of rain events as shown from both radar and distrometer measurements have led us to the classification of rain type into different stages. This results in evolution of Z-R for different type of rain. For a better and realistic model, we present the results from a normalised Gamma DSD fitting, which agrees well with distrometer measurements. We have obtained the statistics of melting layer height and thickness in Singapore and PNG. Finally, we have applied these results in the comparisons of attenuation between radar predicted and measured by the beacon receiver for cases in both Singapore and PNG. The well-agreed results demonstrate the potential of rain characteristics derived from Singapore and PNG for future rain-retrieval algorithms and predicting attenuation methods.

Future work will be focused up the study of the differences in estimated monthly total rainfall between distrometer and raingauge. This is to explore whether tropical raindrops are dominated by lots of small drops. Moreover, we will carry on the study of vertical variation of radar reflectivity and its correlation of

ground rainrates. Additionally, we would like to extend the study of normalised Gamma DSD and to make comparisons with distrometer data from PNG and Chilbolton (UK). Finally, we plan to upgrade Singapore radar in the near future so that we measure differential reflectivity ZDR to derive a better raindrop size distribution from radar data.

Acknowledgement

This project is funded jointly by the UK Radiocommunications Agency, European Union IV Framework (EuroTRMM), ESA/ESTEC and NASDA from Japan. The authors would like to thank Dr T Kozu from Shimane University in Japan, Professor J. T. Ong and Dr K I Timothy at NTU in Singapore, and to UNITECH in PNG for their collaboration. We also gratefully appreciate the team efforts from RCRU staff (J W F Goddard, J D Eastment, D N Ladd and I N Moore) for their useful discussions and successful installation of both Singapore and PNG radar systems.

References

Amitai, E. (1999). "Dependence of Z-R relations on the rain type classification scheme," 29th Intl. Conf. Radar Met., Montreal, Canada, pp 636-639.

Atlas, D., C. W. Ulbrich, and F. D. Marks, (1996): Tropical Rain: Microphysics and radar properties, part II - evaporation and height dependence. *Submitted to J. Appl. Meteor.*

Atlas, D., C. W. Ulbrich, F. D. Marks, E. Amitai, and C. R. Williams, (1998): Systematic variation of drop size and radar - rainfall relations, *Submitted to J. Geophysical Research.*

Black, P. G., J. Proni, J. Wilkerson, and C. Samsury, (1997): Oceanic rainfall detection and classification in tropical and subtropical mesoscale convective systems using underwater acoustic methods. *Mon. Wea. Rev.*, **125**, 2014-2042.

Eastment. J., M. Thurai, D. Ladd, and I. Moore, (1995): A Vertically-Pointing Radar to Measure Precipitation Characteristics in the Tropics. *IEEE Trans. on Geoscience and Remote Sensing*, **33**, No.6, 1336-1340.

Ladd, D. N., C. L. Wilson, and M. Thurai, (1997): Radar Measurements from Papua New Guinea and Their Implications for TRMM PR retrieval algorithms. *IGARS'97*, **IV**, 1648-1650.

Simpson J., R. F. Adler, and G. R. North (1988): A proposed Tropical Rainfall Measuring Mission (TRMM) satellite, Bull. Amer. Meteor. Soc., 69, 278-295.

Testud, J., S Oury, R A Black, P Amayenc and X Dou (2000): The Concept of normalised distribution to describe raindrop spertra: a tool for cloud physics and cloud remote sensing. Submitted to *J. Atmo. Sci.*

Tokay, A., and D. Short, (1996): Evidence from tropical raindrop spectra of the origin of rain from stratiform versus convective clouds. *J.Appl. Meteor.*, **35**, 355-371.